ARTICLE

Dual origin of defect magnetism in graphene and its reversible switching by molecular doping

R.R Nair[1], I-L Tsai[1], M. Sepioni[1], O. Lehtinen[2], J. Keinonen[2], A.V Krasheninnikov[2,3], A.H Castro Neto[4], M.I Katsnelson[5], A.K Geim[1] & I.V Grigorieva[1]

Control of magnetism by applied voltage is desirable for spintronics applications. Finding a suitable material remains an elusive goal, with only a few candidates found so far. Graphene is one of them and attracts interest because of its weak spin–orbit interaction, the ability to control electronic properties by the electric field effect and the possibility to introduce paramagnetic centres such as vacancies and adatoms. Here we show that the magnetism of adatoms in graphene is itinerant and can be controlled by doping, so that magnetic moments are switched on and off. The much-discussed vacancy magnetism is found to have a dual origin, with two approximately equal contributions; one from itinerant magnetism and the other from dangling bonds. Our work suggests that graphene's spin transport can be controlled by the field effect, similar to its electronic and optical properties, and that spin diffusion can be significantly enhanced above a certain carrier density.

[1] Manchester Centre for Mesoscience and Nanotechnology, Manchester M13 9PL, UK. [2] Department of Physics, University of Helsinki, P.O. Box 43, Helsinki FI-00014, Finland. [3] Department of Applied Physics, Aalto University, P.O. Box 11100, Aalto FI-00076, Finland. [4] Department of Physics, Graphene Research Centre, National University of Singapore, 6 Science Drive 2, Singapore 117456, Singapore. [5] Institute for Molecules and Materials, Radboud University of Nijmegen, Nijmegen 6525 AJ, The Netherlands. Correspondence and requests for materials should be addressed to I.V.G. (email: irina.grigorieva@manchester.ac.uk).

Electric field control of magnetic properties has been the subject of considerable attention, with a few materials and hybrid magnetic systems found recently, where it is possible to control the magnetization direction and/or the Curie temperature[1–3]. Electric field tunability is one of the fundamental properties of graphene and has been widely used to control its electronic, optical and other properties related to the electronic structure[4]. On the other hand, graphene is believed to be an ideal material for spintronics[5] because of the weak spin–orbit interaction and long spin relaxation lengths[6,7] and the possibility to introduce paramagnetic centres via controlled introduction of defects, as recent experiments[8,9] have shown that both vacancies and adatoms in graphene carry magnetic moments $\mu \approx \mu_B$. In principle, the latter is not exceptional because defects and impurities in crystals without any d or f elements may have unpaired electrons and, therefore, exhibit paramagnetism[10,11]. However, achieving ferromagnetic alignment between these unpaired spins has proven practically impossible[10]. In graphene, the prospect of defect ferromagnetism is more realistic because, first, the presence of conduction electrons provides a medium for coupling between localized spins and, second, the defect-induced moments are believed to be due to the same π electrons that are responsible for electron transport[12–21]. Accordingly, it should be possible to use the electric-field effect to control not only the coupling between localized magnetic moments in graphene but also the presence of the moments themselves which so far has not been possible in other materials.

In this contribution, we have employed Superconducting Quantum Interference Device (SQUID) magnetometry and molecular doping to investigate graphene's paramagnetism. We have found that magnetic moments due to vacancies and adatoms can be switched off by shifting the Fermi energy E_F above $\approx 0.45\,eV$ and then switched back on by returning to the neutral state or lower E_F. This proves the itinerant nature of magnetic moments in graphene, that is, π magnetism. The localization radius r_L for the itinerant spins is estimated as $\approx 2.0\,nm$. For the case of vacancies, we find them carrying two practically independent moments that are attributed to the π magnetism and an unpaired spin on broken bonds. Only half of vacancy magnetism can be switched off by doping. A profound implication of our findings is that π magnetism can be controlled by other means, notably by the electric field doping within realistically accessible carrier densities $n \approx 2 \times 10^{13}\,cm^{-2}$. Furthermore, it is likely that the unexpectedly quick spin relaxation found in graphene devices and attributed to magnetic defects[22] can be quenched by doping above the above threshold.

Results

Magnetic response of graphene with vacancies. Our samples were graphene laminates that were shown[8] to be a well-characterized, clean reference system, providing enough material (typically, several mg of graphene) for SQUID magnetometry. Our magnetometer (Quantum Design MPMS XL7) allowed measurements at temperatures T between 300 and 1.8 K in fields H up to 7T. The samples were irradiated with 350 keV protons to achieve the desired density of single vacancies, n_v (Methods). Irradiation resulted in a pronounced paramagnetic response arising from non-interacting moments[8]. Typical magnetization curves are shown in Fig. 1. For all vacancy concentrations, such curves were accurately described by the Brillouin function with spin $S = 1/2$. The measured magnetic moment M was found to be proportional to n_v as $M \propto N_S \cdot \mu_B \cdot S \propto n_v$, where μ_B is the Bohr magneton and N_S is the number of spins extracted from Brillouin function fits, in agreement with the earlier report[8].
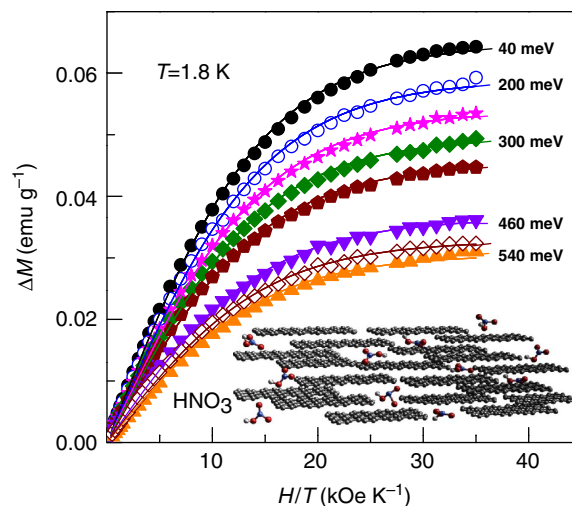

Figure 1 | Effect of hole concentration on vacancy paramagnetism. Symbols show the measured magnetic moment ΔM as a function of magnetic field H for different hole concentrations n. A linear diamagnetic background is subtracted (Methods). Solid curves are fits to the Brillouin function with $S = 1/2$. Labels show the corresponding Fermi energy $|E_F|$ in the valence band. Inset: Illustration of HNO_3 molecules physisorbed in graphene laminates.

Control of carrier concentration in graphene laminates. To probe the evolution of M as the valence (conduction) band gets progressively filled up with holes (electrons), we varied the carrier concentration by using molecular doping: nitric acid (HNO_3) or NO_2 gas as hole dopants[23–25] and aniline as an electron dopant[26]. The properties of HNO_3 and NO_2 as acceptors were investigated both theoretically[24] and experimentally[23,25], and both were shown to be very effective, with each physisorbed molecule resulting in transfer of one electron[25] (see Methods for details). However, finding an effective donor turned out to be problematic. Aniline is reported as one of the best donors but the maximum doping it allowed was only $n \approx 5 \times 10^{12}\,cm^{-2}$. Within the limited range of n achievable for aniline, we have found no difference with respect to hole doping with HNO_3 and, therefore, focus below on the latter results.

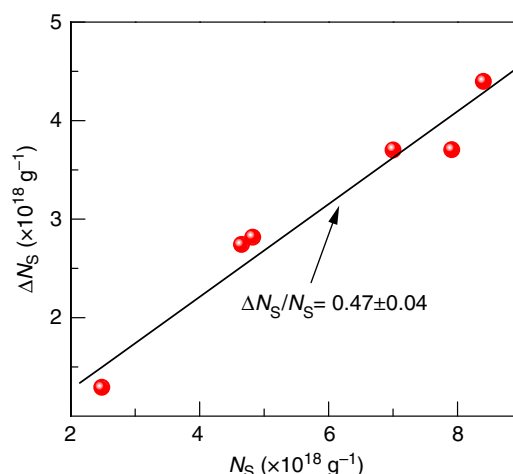**Effect of doping on magnetization of irradiated graphene.** Figure 1 shows the evolution of $M(H)$ curves for one of the irradiated samples as it is doped from a nearly neutral state to $E_F \approx 0.5\,eV$. It is clear that the doping has a strong effect on magnetization: M reduces to half its initial value, even though all $M(H)$ curves look qualitatively the same and are accurately described by the Brillouin function with $S = 1/2$. This indicates a reduction in the number of magnetic moments for the same number of vacancies. It also shows that high n do not lead to stronger interaction, as the vacancy magnetic moments remain noninteracting. This behaviour was found to be universal, even though n_v varied for different samples by more than an order of magnitude, with the average separation between vacancies changing from ~ 3 to 10 nm. Figure 2 shows the evolution of the number of detected spins N_S in two graphene samples with different n_v as a function of E_F. Initially, N_S is gradually decreasing with increasing the hole concentration, but at $E_F \approx 0.4\,eV$, it falls sharply and seems to saturate to $N_S \approx N_S^0/2$ at the maximum doping, where N_S^0 is the number of spins before doping. As soon as the dopants were removed from graphene by mild annealing, M recovered its initial value, that is, the effect is fully reversible (Fig. 2).
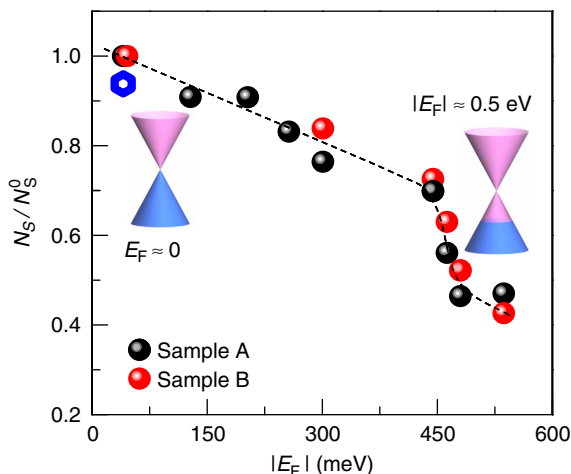
Figure 2 | Reversible control of vacancy magnetism. Normalized density of spins ($S = 1/2$) in two irradiated samples as a function of their doping. N_S^0 is the spin concentration before doping[8], and N_S is extracted from the Brillouin function fit for the $M(H)$ dependence for each doping level, where M is the measured magnetization and H is the applied magnetic field. The dashed curve is a guide to the eye. Open symbol is for sample B after it was maximally doped and then annealed at $\sim 100\,^\circ$C for 2 h. The insets are schematic illustrations of the graphene spectrum in neutral and heavily doped states.


Figure 3 | Universal halving of the vacancy magnetic moment by doping. Symbols show the change in the number of spins after maximum doping, $\Delta N_S = N_S^0 - N_S^f$ in samples with different vacancy concentrations, n_v. N_S^0 is the spin concentration before doping and N_S^f is the number of spins measured at $E_F \geq 0.5$ eV. Solid line is the best fit $\Delta N_S / N_S^0 = 0.47 \pm 0.04$.

$E_F \approx 0.54$ eV was the maximum doping that we were able to achieve with HNO_3, in agreement with the calculated energy dependence of the density of states (DOS) for the NO_2 molecule adsorbed on graphene[24]. The data scatter between different samples and doping levels does not allow us to follow the transition in Fig. 2 in more detail and confirm the apparent saturation to half magnetization above $E_F \approx 0.45$ eV. However, this behaviour was observed for many samples and repeatedly after annealing cycles. To gain further insight, Fig. 3 plots the reduction in magnetization signal at maximum doping, which was measured for several samples with different vacancy densities. It is clear that, independent of the sample and its N_S^0, the 50% reduction in M is universal, as long as the Fermi level is shifted sufficiently away from the neutrality point.

We attribute this finding to the presence of two types of magnetic moments associated with a vacancy, and only one of them is being affected by such a shift in E_F. Indeed, let us recall the origin of defect-induced magnetism in graphene. It lies in the imbalance that the defects create between its two sublattices and the resulting appearance of localized π states with energy close to the Dirac point[12–21]. As long as these states are singly occupied, due to Coulomb repulsion, U_C, they give rise to magnetic moments $\mu = 1\mu_B$. This simple picture is expected for adatoms, such as fluorine or hydrogen, whereas for vacancies the origin of magnetic moments is more complex. In addition to the above π moments, there are dangling σ bonds that can have some role too[14,16,18–21]. For example, vacancies in insulating boron nitride are expected to be magnetic[27]. The relative contribution of σ states to vacancy magnetism is unknown and a matter of debate[18,20]. Because of high chemical reactivity of the dangling bonds, it is often assumed that they are saturated with, for example, hydrogen and therefore do not contribute to magnetism (see, for example, Palacios and Yndurain[18] and Nanda et al.[21]). Then, the magnetic moment is purely due to itinerant (conduction) electrons. Another possible scenario is a vacancy reconstruction and the associated Jan–Teller distortion that results in hybridization between the π and σ states[14,19–21]. Depending on the degree of hybridization, the magnetic moment

for a vacancy has been predicted to be between ~ 1.45 and 2 μ_B (refs 14,16,19,21).

Our experiment suggests an intermediate scenario in which the dangling bonds remain unsaturated and the hybridization does not have a significant role. In this case, each vacancy is expected to provide two independent contributions, which come from the singly occupied localized π state and the unsaturated σ bond. At sufficiently large doping, such that $|E_F| \geq U_C$, the localized π state becomes doubly occupied and the corresponding magnetic moment disappears, whereas the unpaired σ electron remains unaffected by doping and provides the residual M. Because the two contributions appear to be nearly equal, hybridization between the two electronic states should be weak. This is also in agreement with the measured $S = 1/2$. Note that it would require unrealistically high doping to occupy the σ state and fully suppress the vacancy magnetism.

To support the above interpretation, a neat experiment would be to compare the effect of doping on vacancy magnetism with that for adatoms, where there are no dangling bonds and only localized π states are expected[13–15]. However, it has proven difficult experimentally to introduce adatoms without their significant clustering. The latter locally opens a band gap, quenches nearest-neighbour magnetic moments and so on, so that the system can no longer be considered as graphene but becomes its chemical derivative[8]. We have circumvented this problem by exploiting the experimental fact that if graphene is heated at $\geq 350\,^\circ$C, it results in the appearance of so-called resonant scatterers[28–31]. They reduce graphene's electronic quality and result in the D peak in Raman spectra. The scatterers are attributed to some organic residue that is always present on graphene and strongly (sp^3) bonds to it at high T[28]. Resonant scatterers is another name for the localized π states near the Dirac point in the context of electron transport. With these earlier studies in mind, we annealed several samples of pristine (nonirradiated) graphene laminates at $350\,^\circ$C in Ar–H_2 atmosphere. This induced notable paramagnetism with $N_S^0 \approx 3 \times 10^{18}\,g^{-1}$. The observed $M(H)$ curves were practically identical to those of irradiated laminates and, again, are accurately described by the Brillouin function with $S = 1/2$. The found N_S^0 corresponds to 2–3 sp^3 bonds induced by annealing per each graphene crystallite in the laminates.
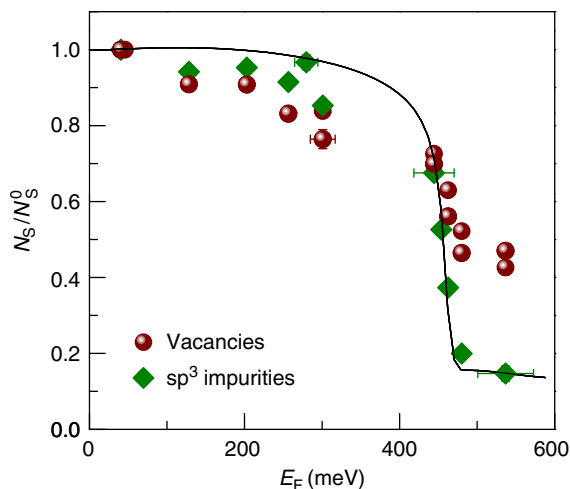
Figure 4 | Fully switchable π magnetism of adatoms. Comparison of the effect of doping on magnetism associated with vacancies (data from Fig. 2) and with sp^3 defects. Solid curve is the theoretical dependence of the normalized number of spins on the Fermi energy, $N_S/N_S^0(E_F)$, calculated using equations (1) and (2), see text. Error bars indicate the accuracy of determination of E_F.

In contrast to vacancy magnetism, the exposure of these sp^3-defected samples to HNO_3 resulted in an almost complete disappearance of the paramagnetic signal above the same $E_F \approx 0.45$ eV (Fig. 4), in agreement with expectations for the purely itinerant nature of sp^3 magnetism. Similar to the case of vacancies, the switching effect is also fully reversible: as soon as HNO_3 molecules were removed by mild annealing at ∼100 °C, the paramagnetic signal recovered its initial value N_S^0.

Discussion

The magnetic moment due to sp^3 impurities and its variation with doping can be calculated analytically using the expression:

$$N(E) = \frac{a^2|E|}{\left[E\left(1 - a^2\ln\left|\frac{E^2}{1-E^2}\right|\right) + E_d\right]^2 + (\pi a^2 E)^2} \quad (1)$$

which describes the DOS in graphene due to resonant scatterers such as sp^3 adsorbates (see Supplementary Note 1). Here, E_d is the states' energy position and a the hybridization parameter, both in units of the half width $W \approx 3t$ of graphene' energy band (t is the nearest-neighbour hopping parameter). For sp^3 impurities relevant to our experiment (monovalent organic groups or hydrogen adatoms), $E_d = 0.02$ and $a = 2/3$ (that is, hybridization strength $\approx 2t$)[31]. The magnetic moment (number of spins) is given by the fraction of singly occupied impurity states, which is determined by the Hubbard energy U and can be found by integrating equation (1) over the occupied states:

$$N_s(E_F) = \int_{E_F - U}^{E_F} dE N(E) \quad (2)$$

Using equation (2), we obtained the $N_S(E_F)$ shown in Fig. 4, which effectively has only one fitting parameter, U, because the dependence is found to be qualitatively insensitive to E_d and a over a wide range of the parameters (the best-fitting value of U as in Fig. 4 is $U = 0.5$ eV). N_S drops sharply at $E_F \approx U$ as expected, exhibiting a cusp-like dependence $1/\ln|E_F - U|$. Note that the cut off does not lead to zero magnetization, which seems surprising but is in agreement with the experiment. The reason for a finite

remaining N_S on the theoretical curve is that the DOS deviates significantly from the standard Lorentzian peak. This arises due to the linear increase in the DOS of conduction electrons in graphene and a renormalization of the positions of impurity states because of hybridization. As a result, $N(E)$ decays as $1/|E|\ln^2|E|$ at large E, much slower than the standard $1/E^2$ dependence for the Lorentz distribution. This means that the magnetic states become totally doubly occupied only for $E_F \gg U$ and, therefore, N_S exhibits a long tail at higher E_F such as in Fig. 4.

Finally, let us add several comments. First, the found value of the Coulomb energy $U = 0.5$ eV allows us to estimate the spatial localization r_L of the π states as $r_L \approx 2.0$ nm (using the known effective Coulomb interactions in graphene[32]), that is, the π state is localized over several benzene rings, in agreement with theory[13,14,16]. Second, comparing the nearly constant N_S at $E_F < 0.3$ eV for sp^3 impurities in Fig. 4 (both theory and experiment) with gradually decreasing N_S for vacancies indicates that the magnetic moment is sensitive to the shape of the DOS peak: the latter is much broader for vacancies[14] resulting in a more gradual decrease of N_S in equation (2), in agreement with experiment. Third, an alternative mechanism for quenching of the magnetic moments at high n could be the Kondo effect[17,20]. However, the observed cumulative contribution from localized and itinerant moments and their T dependence (Supplementary Figs S3 and S4) do not support this scenario (see Supplementary Note 2). Fourth, the discussed threshold doping is achievable in field-effect devices with high-quality gate dielectrics such as boron nitride. This should allow strong suppression of the rapid spin relaxation, characteristic to the existing graphene devices, so that spin currents can be efficiently switched on and off by gate voltage as required for a spin transistor operation.

Methods

to HNO_3 diluted with water at different molar concentrations of 0.1–15 M. The maximum doping level that we could achieve corresponded to $n \approx 2 \times 10^{13}\,cm^{-2}$ or $|E_F| = (\pi n)^{1/2}\hbar v_F \approx 0.54$ eV. Importantly, once exposed to HNO_3, the carrier concentration remained stable for many days at room T, in agreement with relatively high adsorption energy for this molecule[23] but recovered the initial value under mild annealing in argon.

Gaseous NO_2 produced qualitatively similar results (in terms of both measured n and the effect on magnetization), but the doping level was difficult to control and showed significant nonuniformity. Ammonia did not produce any measurable permanent changes in n, presumably because of the difficulty in diffusing ammonia molecules between graphene layers and also much smaller adsorption energy compared with NO_2 (ref. 38). The only donor that produced systematic changes in n was aniline[36], but the maximum possible n was small ($\sim 5 \times 10^{12}\,cm^{-2}$) and resulted in only a small reduction in paramagnetic magnetization, similar to the effect of hole doping at such n. Another known electron dopant N,N,N′,N′-tetramethyl-p-phenylenediamine (TMPD)[39] was found to exhibit weak paramagnetism of its own and, therefore, was avoided.

To monitor the changes in n, we used Hall effect measurements (see Supplementary Fig. S1). They were done on $3 \times 3\,mm^2$ samples cut out of a 2-cm diameter laminate obtained after filtration. The concentration was calculated as $n = I \cdot B/(V_H \cdot e \cdot N_l)$, where I is the applied current, B is the magnetic field, V_H is the Hall voltage and N_l is the number of graphene layers in the laminate. The latter was calculated from the measured sample thickness, typically 3–5 μm, and the average separation between the layers $d \approx 0.36$ nm, as determined using X-ray diffraction.

In addition to the Hall measurements, we used Raman spectroscopy that is also sensitive to n (refs 25,40,41). Raman measurements were carried out using a Renishaw spectrometer with a green laser. As graphene crystallites in the laminates are small (typically 30–50 nm), they produce a significant broadening of all Raman peaks, which makes it difficult to detect exact shifts in their positions that would otherwise yield n. Therefore, we used graphene mechanically exfoliated onto Si/SiO_2 and treated these samples in parallel with graphene laminates used for the Hall and magnetization measurements. Raman spectroscopy on such isolated samples was found to be sufficiently sensitive to detect changes in n even for small changes in HNO_3 concentration.

Examples of Raman spectra after exposure to different concentrations of HNO_3 are shown in Supplementary Fig. S2. We examined the shift and intensity variations of the G peak that is most sensitive to n[25,40,41]. The changes were translated into n by using the calibration data for gated graphene[41]. The absence of the D peak either before or after exposure to HNO_3 (not shown) confirmed that HNO_3 molecules were physisorbed on graphene and not chemisorbed, as the D peak is known to be a measure of short-range defects such as sp^3 bonds[42]. Corresponding Fermi energies for each n were calculated using the relation $E_F = (\pi n)^{1/2}\hbar v_F$, where $v_F = 1.1 \times 10^6\,ms^{-1}$ is the Fermi velocity. We emphasize that the results, shown in Supplementary Fig. S2, are in good agreement with the concentrations obtained from our Hall measurements for the same exposure to HNO_3.

As a further check, we also measured Raman spectra directly on graphene laminates at high doping (HNO_3 concentrations of 11–15 M), where the shift in the G peak position was sufficiently large (peak at 1600–1605 cm^{-1}) to overcome the broadening effect. Again, the results were consistent with the Hall measurements and with the values of n obtained from the Raman spectra on exfoliated monolayers. For these particular measurements, the extracted values of n were in a range of $1–2 \times 10^{13}\,cm^{-2}$.

References

1. Ohno, H. *et al.* Electric-field control of ferromagnetism. *Nature* **408,** 944–946 (2000).
2. Shiba, D. *et al.* Electrical control of the ferromagnetic phase transition in cobalt at room temperature. *Nat. Mater.* **10,** 853–856 (2011).
3. Shiota, Y. *et al.* Induction of coherent magnetization switching in a few atomic layers of FeCo using voltage pulses. *Nat. Mater.* **11,** 39–43 (2012).
4. Geim, A. K. Graphene: status and prospects. *Science* **324,** 1530–1534 (2009).
5. Pesin, D. & MacDonald, A. H. Spintronics and pseudospintronics in graphene and topological insulators. *Nat. Mater.* **11,** 409–416 (2012).
6. Tombros, N., Jozsa, C., Popinciuc, M., Jonkman, H. T. & van Wees, B. J. Electronic spin transport and spin precession in single graphene layers at room temperature. *Nature* **448,** 571–574 (2007).
7. Józsa, C., Popinciuc, M., Tombros, N., Jonkman, H. T. & van Wees, B. J. Controlling the efficiency of spin injection into graphene by carrier drift. *Phys. Rev. B* **79,** 081402(R) (2009).
8. Nair, R. R. *et al.* Spin-half paramagnetism in graphene induced by point defects. *Nat. Phys.* **8,** 199–202 (2012).
9. McCreary, K. M., Swartz, A. G., Han, W., Fabian, J. & Kawakami, R. K. Magnetic moment formation in graphene detected by scattering of pure spin currents. *Phys. Rev. Lett.* **109,** 186604 (2012).
10. Blundell, J. & Pratt, F. L. Organic and molecular magnets. *J. Phys.: Condens. Matter* **16,** R771–R828 (2004).
11. Schlager, H. G. & Löhneysen, H. V. Susceptibility of local magnetic moments in phosphorus-doped silicon near the metal-insulator transition. *Europhys. Lett.* **40,** 661–666 (1997).
12. Lehtinen, P. O., Foster, A. S., Ma, Y., Krasheninnikov, A. V. & Nieminen, R. M. Irradiation-induced magnetism in graphite: a density-functional study. *Phys. Rev. Lett.* **93,** 187202 (2004).
13. Pereira, V. M., Guinea, F., Lopes dos Santos, J. M. B., Peres, N. M. R. & Castro Neto, A. H. Disorder induced localized states in graphene. *Phys. Rev. Lett.* **96,** 036801 (2006).
14. Yazyev, O. V. & Helm, L. Defect-induced magnetism in graphene. *Phys. Rev. B* **75,** 125408 (2007).
15. Uchoa, B., Kotov, V. N., Peres, N. M. R. & Castro Neto, A. H. Localized magnetic states in graphene. *Phys. Rev. Lett.* **101,** 026805 (2008).
16. Palacios, J. J., Fernández-Rossier, J. & Brey, L. Vacancy-induced magnetism in graphene and graphene ribbons. *Phys. Rev. B* **77,** 195428 (2008).
17. Haase, P., Fuchs, S., Pruschke, T., Ochoa, H. & Guinea, P. Magnetic moments and Kondo effect near vacancies and resonant scatterers in graphene. *Phys. Rev. B* **83,** 241408 (2011).
18. Palacios, J. J. & Yndurain, F. Critical analysis of vacancy-induced magnetism in monolayer and bilayer graphene. *Phys. Rev. B* **85,** 245443 (2012).
19. Santos, E. J. G., Riikonen, S., Sánchez-Portal, D. & Ayuela, A. Magnetism of single vacancies in rippled graphene. *J. Phys. Chem. C* **116,** 7602–7606 (2012).
20. Cazalilla, M. A., Iucci, A., Guinea, F. & Castro Neto, A. H. Local moment formation and Kondo effect in defective graphene. *Preprint arXiv* **1207,** 3135 (2012).
21. Nanda, B. R. K., Sherafati, M., Popović, Z. S. & Satpathy, S. Electronic structure of the substitutional vacancy in graphene: density-functional and Green's function studies. *New J. Phys.* **14,** 083004 (2012).
22. Lundberg, M. B., Yang, R., Renard, J. & Folk, J. A. Defect-mediated spin relaxation and dephasing in graphene. *Phys. Rev. Lett.* **110,** 156601 (2013).
23. Bae, S. *et al.* Roll-to-roll production of 30-inch graphene films for transparent electrodes. *Nat. Nanotechnol.* **5,** 574–578 (2010).
24. Wehling, T. O. *et al.* Molecular doping of graphene. *Nano Lett.* **8,** 173–177 (2008).
25. Crowther, A. C. *et al.* Strong charge-transfer doping of 1 to 10 layer graphene by NO_2. *ACS Nano* **6,** 1865–1875 (2012).
26. Liu, H., Liu, Y. & Zhu, D. Chemical doping of graphene. *J. Mater. Chem.* **21,** 3335–3345 (2011).
27. Du, A. *et al.* Dots versus antidots: Computational Exploration of structure, magnetism, and half-metallicity in boron-nitride nanostructures. *J. Am. Chem. Soc.* **131,** 17354–17359 (2009).
28. Ni, Z. H. *et al.* On resonant scatterers as a factor limiting carrier mobility in graphene. *Nano. Lett.* **10,** 3868–3872 (2010).
29. Yung-Chang, L. *et al.* Graphene annealing: How clean can it be? *Nano. Lett.* **12,** 414–419 (2012).
30. Jieun, S., Yeoung, K. T. & Sunmin, R. Raman spectroscopy study of annealing-induced effects on graphene prepared by mechanical exfoliation. *Bul. Korean Chem. Soc.* **31,** 2679–2682 (2010).
31. Wehling, T. O., Yuan, S., Lichtenstein, A. I., Geim, A. K. & Katsnelson, M. I. Resonant scattering by realistic impurities in graphene. *Phys. Rev. Lett.* **105,** 056802 (2010).
32. Wehling, T. O., Şaşioğlu, E., Friedrich, C., Lichtenstein, A. I. & Katsnelson, M. I. Effective Coulomb interactions in graphene and graphite. *Phys. Rev. Lett.* **106,** 236805 (2011).
33. Sepioni, M. *et al.* Limits on intrinsic magnetism in graphene. *Phys. Rev. Lett.* **105,** 207205 (2010).
34. Lehtinen, P. O. *et al.* Magnetic properties and diffusion of adatoms on a graphene sheet. *Phys. Rev. Lett.* **91,** 017202 (2003).
35. Schedin, F. *et al.* Detection of individual gas molecules adsorbed on graphene. *Nat. Mater.* **6,** 652–655 (2007).
36. Dong, X. *et al.* Doping single-layer graphene with aromatic molecules. *Small* **5,** 1422–1426 (2009).
37. Das, B., Voggu, R., Rout, C. S. & Rao, C. N. R. Changes in the electronic structure and properties of graphene induced by molecular charge-transfer. *Chem. Commun.* 5155–5157 (2008).
38. Leenaerts, O., Partoens, B. & Peeters, F. M. Adsorption of H_2O, NH_3, CO, NO_2 and NO on graphene: a first-principles study. *Phys. Rev. B* **77,** 125416 (2008).
39. Dettlaff-Weglikowska, U., Kim, G., Bulusheva, L. G. & Roth, S. Modification of the electronic structure in single-walled carbon nanotubes with aromatic amines. *Physica Status Solidi B* **248,** 2458–2461 (2011).
40. Pisana, S. *et al.* Breakdown of the adiabatic Born–Oppenheimer approximation in graphene. *Nat. Mater* **6,** 198–201 (2007).
41. Das, A. *et al.* Monitoring dopants by Raman scattering in an electrochemically top-gated graphene transistor. *Nat. Nanotechnol.* **3,** 210–215 (2008).
42. Elias, D. C. *et al.* Control of graphene's properties by reversible hydrogenation: evidence for graphane. *Science* **323,** 610–613 (2009).

Author contributions

I.V.G. directed the project. I.V.G. and R.R.N. designed the experiments. R.R.N., I.-L.T. and M.S. performed the experiments. O.L., J.K. and A.V.K. performed proton irradiation and analysed defect structures. M.I.K. and A.H.C.N. provided theory. I.V.G. and A.K.G. wrote the paper. All authors contributed to discussions of the results.

Additional information

Supplementary Information accompanies this paper at http://www.nature.com/naturecommunications

Competing financial interests: The authors declare no competing financial interests.

Reprints and permission information is available online at http://npg.nature.com/reprintsandpermissions/

How to cite this article: Nair, R. R. *et al.* Dual origin of defect magnetism in graphene and its reversible switching by molecular doping. *Nat. Commun.* 4:2010 doi: 10.1038/ncomms3010 (2013).
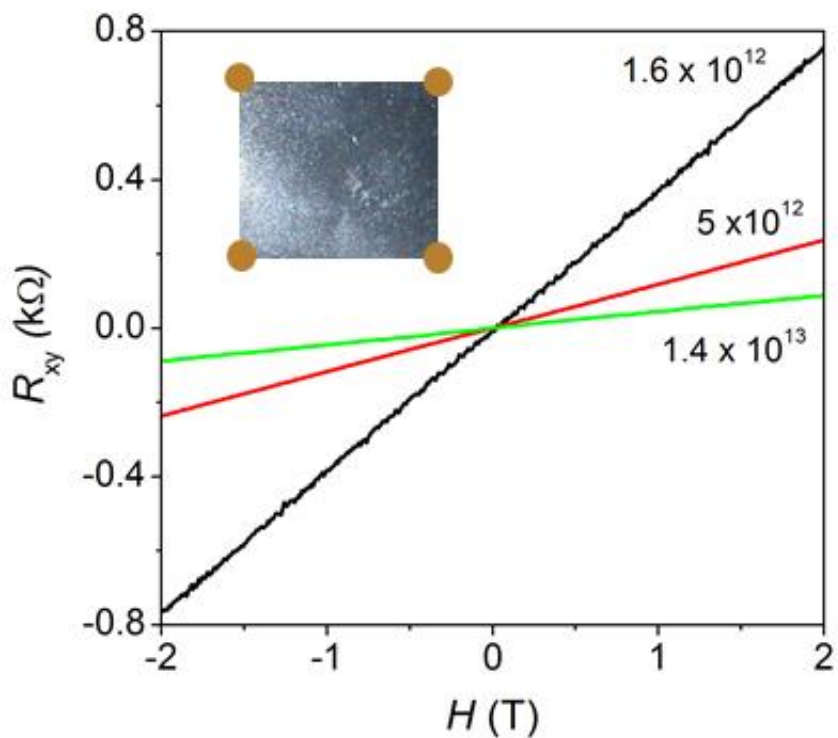
**Supplementary Figure S1. Carrier concentrations in doped graphene laminates.** Hall resistance per graphene layer in the laminate (R_{xy}) as a function of applied magnetic field for HNO_3 doped graphene. Labels show corresponding carrier concentrations in cm^{-2}. *Inset*: Hall measurements were carried out in the van-der-Pauw geometry on 3×3 mm samples cut out of a 2 cm-diameter laminate obtained after filtration.
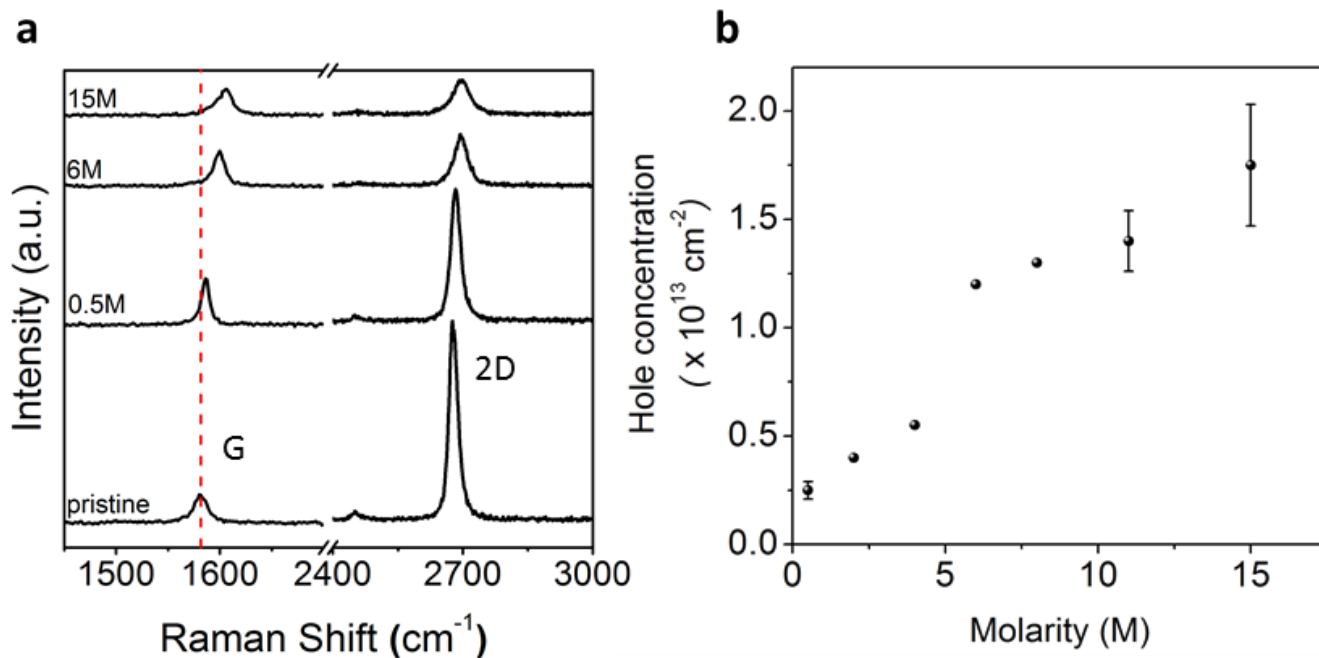
Supplementary Figure S2. Evolution of Raman spectra with doping. a – Examples of Raman spectra of monolayer graphene mechanically exfoliated onto Si/ SiO$_2$ substrate and exposed to nitric acid at different concentrations; labels show molar concentrations of HNO$_3$. Corresponding G-peak positions are 1581±0.5, 1586±0.5, 1599±0.5 and 1603±1 cm^{-1}. b – Carrier concentrations as a function of molar concentration of HNO$_3$ found from the G peak positions.
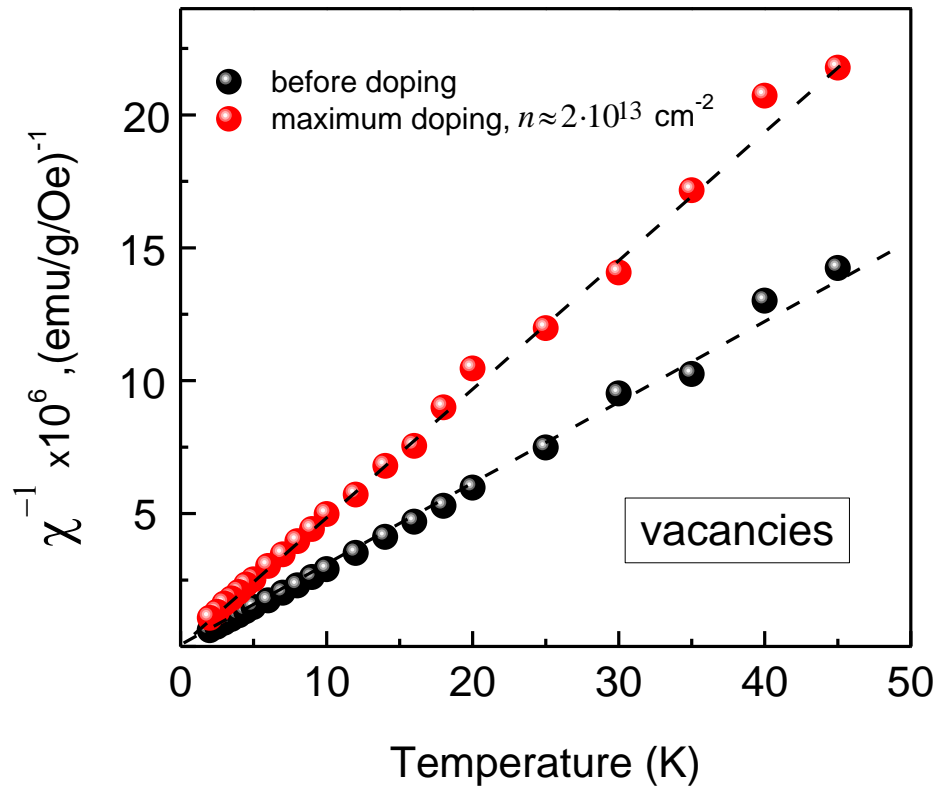
Supplementary Figure S3. Absence of deviations from the Curie law for graphene with vacancies. Inverse paramagnetic susceptibility for an irradiated sample also used in the main text. Measurements were done in parallel field $H = 3$ kOe. Constant diamagnetic background subtracted.
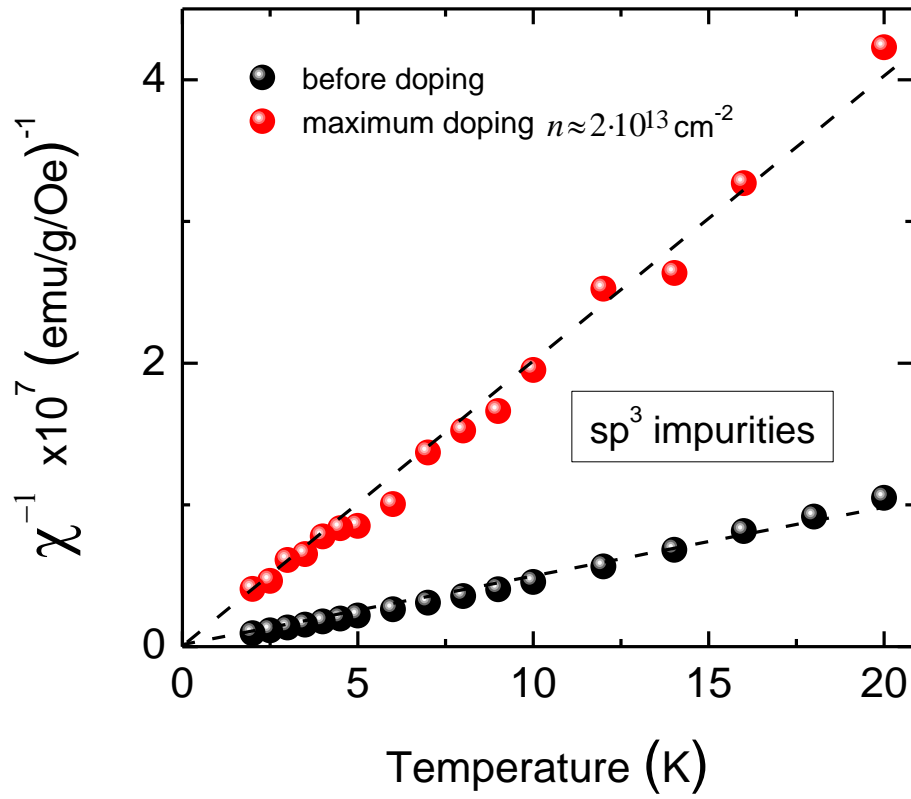
Supplementary Figure S4. Absence of deviations from the Curie law for graphene with sp^3 impurities. Inverse paramagnetic susceptibility for a sample containing sp^3 impurities. This sample was heat-treated at 350°C (see main text). Measurements were done in parallel field H = 5 kOe. Constant diamagnetic background subtracted.

Supplementary Note 1. Calculation of the density of states for graphene with sp^3 impurities

The simplest description of the electronic structure of adsorbates covalently bound to carbon atoms in graphene is based on the hybridization model, where two types of electronic states are postulated: localized (responsible for the formation of mid-gap states) and itinerant, or conduction electron states [15,31,43,44]. For the hybridization model the Green's function of the localized states can be expressed as

$$G_d(E) = \frac{1}{E - E_d - \sum_k \frac{|V_k|^2}{E - t(k)}} \qquad (S1)$$

where $t(k)$ is the band-electron dispersion, V_k is the momentum-dependent hybridization parameter (see Ref. [43], Eq.(17)) and E_d is the states' energy position. Assuming for simplicity $V_k = V = const$ we find

$$G_d(E) = \frac{1}{E - E_d - V^2 g_0(E)} \qquad (S2)$$

where $g_0(E)$ is the on-site Green's function of conduction electrons for an ideal crystal (see Ref. [43], Eq.(6)). For the latter we have chosen a simplified model of the electron energy spectrum with the linear-in-energy density of states cut at the half-bandwidth ("graphene" model of Ref. [43]). Thus, we have:

$$N(E) = -\frac{1}{\pi} \operatorname{Im} G_d(E) = \frac{a|E|}{\left[E\left(1 - a\ln\left|\frac{E^2}{1-E^2}\right|\right) + E_d \right]^2 + (\pi a E)^2} \qquad (S3)$$

where energies E, E_d are expressed in terms of the half-bandwidth, $D = 3t$, $a = (V/D)^2$.

Supplementary Note 2. Temperature dependence of magnetic susceptibility and remarks on Kondo effect

The central result of our study is the observation of quenching of defects' magnetic moments at sufficiently high doping, where the Fermi level is shifted to $E_F \geq 0.45$ eV. We attribute this effect to double occupation (with both up and down spins) of the localised states created by the defects (see main text). An alternative explanation of this effect could be the much-discussed Kondo effect in graphene [17,20,45-47]. The Kondo effect in irradiated graphene was claimed by Chen et al [45] on the basis of the observed logarithmic corrections to the resistivity of ion-irradiated graphene samples. However, the same experimental data allow an alternative explanation based on weak localization corrections [46,47]. Also, the *s-d* exchange coupling between localized and conduction electron spins has been shown to be *ferromagnetic*, i.e. the alignment of the localized and conduction electron spins is expected to be parallel [17], which rules out the Kondo effect.

Irrespective of this theoretical work, our experimental observation that the spins of localized (σ-band) and itinerant (π-band) electrons do not cancel each other shows that they are, indeed, *parallel*.

In addition, the Kondo effect – if relevant - would show up in magnetisation measurements as deviations of the *T* dependence of the magnetic susceptibility χ from the Curie law $\chi \propto 1/T$, at *T* below the Kondo temperature [48]. Therefore, to distinguish between quenching of the magnetic moments due to doping and due to possible Kondo effect, we measured $\chi(T) = M(T)/H$, for both types of studied defects (vacancies and sp^3 impurities). Here $M(T)$ is the measured magnetic moment and *H* the applied field. Supplementary Fig. S3 shows the results for one of the irradiated samples and Supplementary Fig. S4 for a sample with sp^3 defects. In both cases the Curie law holds accurately down to 2K, the lowest *T* in our experiments, without any noticeable offset from zero. This also contradicts the existence of antiferromagnetic coupling (corresponding to the Kondo effect). Therefore, our data clearly do not support the Kondo scenario.

Supplementary References

43. Wehling, T.O. Katsnelson, M. I. Lichtenstein, A.I. Adsorbates on graphene: Impurity states and electron scattering. *Chem. Phys. Lett.* **476**, 125-134 (2009).

44. Robinson, J. P. Schomerus, H. Oroszlány, L. & Fal'ko, V. I. Adsorbate-limited conductivity of graphene. *Phys. Rev. Lett.* **101**, 196803 (2008).

45. Chen, J-H., Li, L., Cullen, W.G., Williams, E. D & Fuhrer, M. S. Tunable Kondo effect in graphene with defects. *Nature Physics* **7**, 535-538 (2011).

46. Jobst, J. and Weber, H.B. Origin of logarithmic resistance correction in graphene. *Nature Physics* **8**, 352 (2012).

47. Chen, J-H., Li, L., Cullen, W.G., Williams, E. D & Fuhrer, M. S. Reply to "Origin of logarithmic resistance correction in graphene" *Nature Physics* **8**, 353 (2012).

48. Hewson, A. C. *The Kondo Problem to Heavy Fermions* (Cambridge University Press, Cambridge, 1993).